Biophysical techniques to distinguish ligand binding modes in cytochrome P450 monooxygenases

Matthew N. Podgorski,[†,⊥] Joshua S. Harbort,[‡,⊥] Tom Coleman, [†,⊥] Jeanette E. Stok,[¶] Jake A. Yorke,[∫] Luet-Lok Wong,[∫] John B. Bruning,[Δ] Paul V. Bernhardt,*[,¶]James J. De Voss, *[,¶] Jeffrey R. Harmer*[,‡] and Stephen G. Bell*[,†]

[†] Department of Chemistry, University Adelaide, Adelaide, SA, 5005, Australia.

[‡] Center for Advanced Imaging, University of Queensland, Brisbane, QLD, 4072, Australia.

[¶] School of Chemistry and Molecular Bioscience, University of Queensland, Brisbane, QLD, 4072, Australia.

[∫] Department of Chemistry, University of Oxford, Inorganic Chemistry Laboratory, South Parks Road, Oxford, OX1 3QR, UK.

[Δ]School of Biological Sciences, University of Adelaide, SA 5005, Australia

ABSTRACT: The cytochrome P450 superfamily of heme monooxygenases catalyze important chemical reactions across nature. The changes in the optical spectra of these enzymes, induced by the addition of substrates or inhibitors, are critical for assessing how these molecules bind to the P450, enhancing or inhibiting the catalytic cycle. Here we use the bacterial CYP199A4 enzyme (Uniprot ID; Q2IUO2), from *Rhodopseudomonas palustris* HaA2, and a range of substituted benzoic acids to investigate different binding modes. 4-Methoxybenzoic acid elicits an archetypal type I spectral response due to a ≥95% switch from the low- to high-spin state with concomitant dissociation of the sixth aqua ligand. 4-(Pyridin-3-yl)- and 4-(pyridin-2-yl)-benzoic acid induced different type II UV-vis spectral responses in CYP199A4. The former induced a greater red shift in the Soret wavelength (424 versus 422 nm) along with a larger overall absorbance change and other differences in the α-, β- and δ-bands. There were also variations in the ferrous UV-vis spectra of these two substrate-bound forms with a spectrum indicative of Fe-N bond formation with 4-(pyridin-3-yl)benzoic acid. The crystal structures of CYP199A4, with the pyridinyl compounds bound, revealed that while the nitrogen of 4-(pyridin-3-yl)benzoic acid is coordinated to the heme, with 4-(pyridin-2-yl)benzoic acid an aqua ligand remains. Continuous wave and pulse EPR data in frozen solution revealed that the substrates are bound in the active site in a form consistent with the crystal structures. The redox potential of each CYP199A4-substrate combination was measured, allowing correlation between binding modes, spectroscopic properties and the observed biochemical activity.

Introduction

The cytochrome P450 (CYP) superfamily of heme-thiolate monooxygenase enzymes can catalyze the insertion of an oxygen atom into an unactivated C-H bond as well as a wide range of other chemical transformations.[1-3] These are essential biological functions, which are difficult to carry out chemically, but impressively these enzymes perform these reactions under ambient conditions, often with high selectivity and activity. The first step of the archetypal P450 catalytic cycle is usually substrate binding to the six coordinate (Cys-aqua) ferric heme resting state, which results in the expulsion of the distal aqua ligand. This allows efficient transfer of the first electron and commencement of the catalytic cycle.[4-9] Oxygen binding is the next step and the ferrous dioxy-bound form then undergoes a second single electron reduction followed by oxygen activation to generate the active oxidant, the ferryl Compound I (Cpd I) intermediate.[10-15] The hydroxylation reaction then proceeds via the radical rebound mechanism of Groves and McClusky.[16, 17]

Ligand binding to a P450 is not only crucial for initiating the catalytic cycle but tight binders that aren't substrates are effective inhibitors of these enzymes.[4, 18-20] It has been postulated that this inhibition arises not only from competitive inhibition of substrate binding but can also involve a change in the redox potential of the P450, effectively preventing formation of the ferrous heme.[18-20] Many of the azole anti-fungal drugs act by binding tightly to P450s that are essential for steroid formation in fungi.[21] In addition, competition by different P450 xenobiotics involved in human metabolism is believed to be responsible for many drug-drug interactions.[22] Given these observations, it is not surprising that many biophysical techniques have been used to assess ligand affinity and binding mode e.g. active site and/or heme ligation. The most common technique is UV-vis optical spectroscopy but X-ray crystallography, EPR spectroscopy and more recently, spectroelectrochemistry experiments, which combines UV-vis spectroscopy with redox potential determination, are also used. [23, 24,25, 26]

A ferric P450 heme can be high-spin (HS, $S = 5/2$), or low-spin (LS, $S = 1/2$), and these electronic ground states can be distinguished by optical and EPR spectra.[26-33] The UV-vis spectrum of a substrate-bound cytochrome P450 is dependent on the nature of heme ligation. A type I change (blue shift; ~418 nm to ~390 nm) is associated with an increase in HS character upon ligand binding to the enzyme, whereas a reverse type I spectral change (red shift; ~390 nm to ~418 nm) reflects a change from more HS to LS character. A type II difference spectrum (red shift; typically ~418 nm to ~420-424 nm) is indicative of ligand

binding to the heme or perturbation of the environment of the heme-bound ligand (see below) and arises as a result of a stronger axial ligand field. Type II spectra have been subdivided into two types: IIa reflects a shift from the HS to LS form whereas IIb reflects a LS to LS state switch but with a stronger ligand field.[27] Ligands which bind in type II fashion are often nitrogen-donor inhibitors as they prevent reduction and coordination of dioxygen. When assessing the heme bound ligands of P450cam (CYP101A1) Dawson and co-workers found differences in the spectral shifts with different nitrogen containing ligands and classified these as "normal" or "abnormal" donor shifts.[29] Such inhibitors have profoundly important bioactivities: for example, the azole antifungal drugs function by type II binding to and inhibition of P450s involved in sterol biogenesis.

Recent results have highlighted that type II shifts are more complex than first thought.[23, 24, 34-36] For example the extent of the red-shift of the Soret band in the spectrum (λ_{max}) is known to be dependent on the electronic properties of the N-donor ligand but this relationship is poorly defined. Therefore, it is not always clear whether the different λ_{max} values are due to restraints that alter the nitrogen-iron interaction, electronic effects, a population of the substrate binding in different conformations, or a combination of these factors. Type II shifts have also been reported for nitrogen containing ligands which do not directly coordinate to the heme but interact noncovalently with the heme aqua ligand and these interactions do not always lead to inhibition of catalytic activity.[23] This binding mode in various P450 enzymes has been investigated using continuous wave (CW) and pulse EPR spectroscopy.[26, 28, 32, 33, 37-40] Given the importance of substrate/inhibitor binding to P450s and the different modes available we have used a set of biophysical measurements to characterize selected binding modes in a single enzyme system.

The cytochrome P450 monooxygenase, CYP199A4 from *Rhodopseudomonas palustris* HaA2 (Uniprot ID; Q2IUO2), has a high affinity for *para*-substituted benzoate substrates.[7, 8, 41-44] It is able to bind and demethylate 4-methoxy- and 4-methylaminobenzoic acids, while 4-ethylbenzoic acid is hydroxylated and desaturated to form alcohol and alkene products.[7, 42, 44] The oxidation activity of CYP199A4 for these substrates, which is supported by a ferredoxin reductase (HaPuR) and a [2Fe-2S] ferredoxin (HaPux), is high.[7, 45] The selectivity of CYP199A4 for oxidation at the *para*-substituent is also high. As with P450cam, the binding of a substrate which displaces the aqua ligand and changes the spin state, has been shown to be a critical factor for efficient transfer of the first electron to CYP199A4 and commencement of the catalytic cycle. This step is also associated with a significant change in the redox potential of the heme.[4, 5, 46] Structural analyses of the substrate-bound forms of CYP199A4 have been undertaken[7, 43, 45, 47] and these crystal structures explain the preference of CYP199A4 for attack at the *para*-substituent.[7, 43, 45] They highlight that the benzoate moiety is held in the substrate binding pocket by both hydrophilic and hydrophobic interactions. Modification of the substrate benzoate moiety greatly diminishes binding affinity but replacement at the *para*-substituent carboxylate with alternate functional groups is possible.[7-9, 44, 45] Consistent with the ≥95% spectral type I shift to the HS form observed when 4-methoxybenzoic acid binds, the *para*-methoxy group is held in proximity to the heme (the methyl group is 4.1 Å from the iron) and the aqua ligand is displaced (PDB: 4DO1).[43] Therefore changing the *para*-moiety allows facile positioning of different substituents close to the heme.

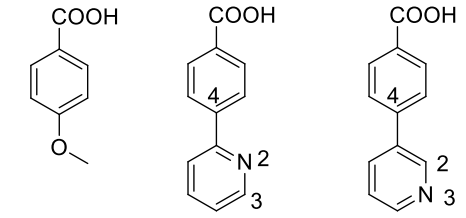

4-methoxy-benzoic acid | 4-(pyridin-2-yl)-benzoic acid | 4-(pyridin-3-yl)-benzoic acid

Figure 1 CYP199A4 substrates investigated in or relevant to this study. The numbering system, relevant for the naming or the pyridinyl benzoic acids, is highlighted. In this system the 4 in all substrates refers to the *para*-substituent of the benzoic acid. In the pyridinyl benzoic acids the 2 and 3 numbering refers to the *ortho* or *meta* relationship of the pyridinyl nitrogen to the benzoic acid group.

As a result of this CYP199A4 is suitable for studies comparing different cytochrome P450 binding modes using substrates with different nitrogen containing moieties at the *para*-position. Here we investigate how two pyridinyl substituted benzoic acids, which could act as inhibitors of the enzyme, bind to CYP199A4 (Figure 1). The crystal structures of CYP199A4 with these substrates were determined to provide insight into the different substrate binding modes and spectral responses observed. Optical spectroelectrochemical determination of the redox potential of CYP199A4 in the presence of each substrate/inhibitor was undertaken, providing further correlation between binding mode and different physicochemical properties.

Experimental Details

Redox potential determination

Optical electrochemistry utilized a Pine Instruments quartz spectroelectrochemical cell comprising a combination Pt 'honeycomb' working electrode and Pt auxiliary electrode with a separate Ag/AgCl reference electrode. The optical path length was 1.7 mm. The reference electrode was calibrated with quinhydrone (E' +285 mV vs NHE at pH 7). The solutions were approximately 20 μM in CYP199A4 (in Tris buffer (50 mM, pH 7.4). To avoid interference from highly colored organic meditators each experiment contained 20 μM of the complexes $[Co(AMMEN_3S_3sar)]^{5+}$, $[Co(CLMEN_4S_2sar)]^{3+}$, $[Co(AMMEN_5Ssar)]^{3+}$, $[Co(sep)]^{3+}$, $[Co(AMMEsar)]^{3+}$, $[Co(cis\text{-}diammac)]^{3+}$ and $[Co(trans\text{-}diammac)]^{3+}$ (see Supporting Information) which provided redox buffering across the potential range $0 < E_h < -600$ mV vs NHE. [48, 49] These complexes have small molar extinction coefficients ($\varepsilon < 300$ $M^{-1}cm^{-1}$) so they make no significant contribution to the visible spectra at micromolar concentrations.

Potential dependent absorption spectra were acquired across the range 370 to 800 nm within an anaerobic glovebox (O_2 < 20 ppm) with an Ocean Optics USB2000 fiber optic spectrophotometer and a DT-MINI-2-GS miniature deuterium/tungsten/halogen UV-Vis-NIR light source. Potentials were set with a BAS100B/W potentiostat operating in constant potential electrolysis mode and absorption spectra acquired when all absorbance changes ceased (typically within 10 min). Spectra were taken at 25 mV intervals and reversibility was established by stepping the potential firstly in negative and then in positive di-

rections. No significant hysteresis was found. Data were modeled by global analysis of the potential dependent absorbance spectra (all wavelengths) with Reactlab Redox[50] using a single electron transfer model (equation 1).

$$Abs(E) = \frac{Abs_{max}}{1 + 10^{\frac{E-E1}{59}}} \quad (1)$$

The measurement and analysis of redox potentials using organic mediators was performed as described previously.[46, 51]

Protein crystallization and X-ray crystallography

For crystallization, CYP199A4 was further purified by size exclusion chromatography (HiPrep Sephacryl S-200 HR 16 x 600 mm, GE Healthcare). For both pyridinyl compounds a co-concentration method was used to obtain crystals. 4-(Pyridin-3-yl)benzoic acid or 4-(pyridin-2-yl)benzoic acid (3 mM) from a 100 mM stock solution in 100% DMSO was added to dilute protein (~10 μM). The mixture was incubated at 4 ˚C for 2 hours, and the protein-ligand complex was then concentrated to 30-40 mg mL^{-1}. Crystals were obtained using the hanging-drop vapor diffusion method at 16 ºC using 1 μL of protein with 1 μL of reservoir solution and equilibrated with 500 μL of the same reservoir solution. Clusters of red plate-like crystals appeared within half a day to one week from 30-40 mg mL^{-1} CYP199A4 with a reservoir solution containing 0.2 M magnesium acetate tetrahydrate, 20-32% w/v PEG-3,350 and 0.1 M Bis-Tris pH 5.0-5.75.

Crystals were harvested using a Microloop or Micromount (MiTeGen), then cryoprotected by immersion in Parabar 10312 (Paratone-N, Hampton Research) and flash cooled in liquid N_2. X-ray diffraction data was collected at 100 K on the MX1 beamline at the Australian Synchrotron.[52, 53] All diffraction data were indexed and integrated using iMosflm;[54] scaled, merged and R-free flags were added using Aimless,[55] both available in the CCP4 suite of programs.[56] The phase problem was solved using the molecular replacement method with Phaser in CCP4,[57] using CYP199A4 (PDB: 5UVB, with the substrate and heme removed) as the initial search model. Electron density maps were obtained after initial model building and the model was rebuilt using Coot.[58] Structural refinements were performed over multiple iterations using Phenix Refine available in the Phenix suite of programs.[59] Composite omit maps were generated using the composite omit maps program in Phenix. Data collection and structural refinement statistics for the data sets are summarized in the Supporting Information. The coordinates for the crystal structures of the substrate-bound CYP199A4 have been deposited in the Protein Data Bank.

EPR spectroscopy

Sample preparation. P450 samples used for EPR experiments were expressed in *E. coli* as described earlier and purified in buffer with 10-20% cryoprotectant glycerol to a final P450 concentration of ~500 μM. 4-Methoxybenzoic acid was dissolved in ethanol to a concentration of 100 mM and added to CYP199A4 solution for a final substrate concentration of ≈1000 μM. 4-(Pyridin-2-yl)benzoic acid and 4-(pyridin-3-yl)benzoic acid were less soluble in ethanol and so were dissolved instead in DMSO (to 100 mM) and added to CYP199A4 solution for a final concentration of ≈1200 μM. The pyridine substrates were incubated in a 4°C fridge, for ~12 hours for 4-(pyridin-2-yl)benzoic acid, and for ~24 hours for 4-(pyridin-3-yl)benzoic acid before freezing. Samples were transferred to EPR tubes and frozen rapidly in liquid nitrogen for EPR measurement. *CW EPR.* X-band CW EPR spectra were measured at 15 K on a Bruker E500 (Bruker E580) spectrometer equipped with a Bruker super-high Q spherical CW EPR resonator (a Bruker 4 mm ENDOR resonator model EN4118X-MD4) and liquid helium cryostat (from Oxford Instruments or a cryogen-free variable temperature cryostat from Cryogenic Ltd, model PT415). CW EPR data was measured with a modulation amplitude of 0.5 mT, a 100 kHz modulation frequency, and under non-saturating conditions. The magnetic field was calibrated with 2,2-diphenyl-1-picrylhydrazyl (DPPH), g = 2.0036. *Pulsed EPR.* Pulse X-band EPR spectra were measured on a Bruker E580 spectrometer using a 1 kW TWT microwave amplifier and a Bruker 4 mm ENDOR resonator, model EN4118X-MD4. The pulse sequences used are as follows. *HYSCORE,* $\pi/2$ - τ - $\pi/2$ - t_1 - π - t_2 - $\pi/2$ - τ – echo using mw pulse lengths of $t_{\pi/2}$ = 16 ns, t_π = 16 ns, with starting times 48 ns, time increments 20 ns, a repetition rate 765 μs, observer field positons 295-297 mT, and τ values 144 -152 ns. An eight-step phase cycle was used. Blind-spots were checked for by comparing spectra measured with different τ values. The time traces were baseline corrected with an exponential, apodized with a Gaussian window, and zero-filled. After a two-dimensional Fourier transformation, absolute-value spectra were calculated. *X-Band Mims ENDOR,* $\pi/2$ - τ - $\pi/2$ - T_{RF} - $\pi/2$ – echo using mw pulse lengths of $t_{\pi/2}$ = 14 ns, a selective radiofrequency (rf) pulse of variable frequency and length (between 9 μs to 16 μs) applied during the time interval T_{RF}. Spectra were measured at 12.5 K using a repetition time of 1 to 1.5 ms using a 150 W or 500 W rf amplifier (Amplifier Research, model 150A400 and model 500A250C). Blind spots were checked for by comparing spectra measured with τ values of 82 ns and 142 ns. *Data Processing and EPR Simulations.* EPR data were processed using MATLAB 8.5.0.197613 (R2015a) (The MathWorks, Inc.). Simulations were performed using EasySpin[60] and XSophe-Sophe-XeprView[61]

Results

Assessment of substrate binding by UV-vis spectroscopy

Substrate binding to cytochrome P450 enzymes can be conveniently measured by monitoring the UV-vis absorbance spectrum upon addition of the compound of interest.[27, 29, 62] Both 4-(pyridin-2-yl)- and 4-(pyridin-3-yl)-benzoic acids induced type II spin state shifts in CYP199A4 (Figure 2). However, 4-(pyridin-3-yl)benzoic acid induced a greater shift in the λ_{max} (λ_{max}: 424 versus 422 nm) and there were distinguishable differences between the spectra in the region of the α/β bands (Figure 2, Table S1 and Figure S1). The modifications on the addition of these substrates were more apparent in the difference spectra (Figure 2 and Figure S1). The peak and trough for 4-(pyridin-2-yl)benzoic acid are at 430 and 412 nm, respectively, while those for 4-(pyridin-3-yl)benzoic acid are at 432 and 414 nm. With 4-(pyridin-3-yl)benzoic acid there was a greater decrease in the Soret band trough as well as a significant lowering of the absorbance in the region corresponding to the α band (at 570 nm). There was also an increase in absorbance at ~372 nm. The peak-to-trough absorbance difference was smaller with 4-(pyridin-2-yl)benzoic acid and the α/β band region increased slightly in intensity (at 577 nm). The differences in the spectral shifts with 4-(pyridin-3-yl)benzoic acid were reminiscent of those

Table 1 Substrate/inhibitor binding and *in vitro* turnover data for CYP199A4 with 4-methoxybenzoic acid, 4-(pyridin-2-yl)benzoic acid and 4-(pyridin-3-yl)benzoic acid.

Substrate	HS %	K_d (μM)	$E_{m,8}$ [b] (V vs NHE)	NADH	PFR	Coupling (%)[d]
4-methoxyBA[a]	>95	0.28 ± 0.01	-0.188	1340 ± 28	1220 ± 120	91 ± 2
4-(pyridin-2-yl)BA	Type II 422 nm	1.0 ± 0.1	-0.462	9.8 ± 2.1	-[c]	-[c]
4-(pyridin-3-yl)BA	Type II 424 nm	2.3 ± 0.1	-0.321	30.0 ± 2.8	-[c]	-[c]
substrate-free	-	-	-0.438	9.0	-	-

[a] Data published previously.[7, 43] [b] All the redox potentials are presented with a precision of +/- 10 mV [c] No product formation. [d] Hydrogen peroxide uncoupling was measured for 4-methoxybenzoic acid oxidation and made up ≤2.5% of the added NADH.

The data for 4-methoxybenzoic acid, which have previously been reported (except the redox potential), are provided for comparison. The NADH oxidation rate is the frequency of NADH oxidation, including product formation and uncoupling reactions. PFR is the product formation rate; the coupling efficiency is defined as the percentage of NADH utilized for the formation of products. The turnovers were measured using a HaPuR:HaPux:CYP199A4 concentration ratio of 1:10:1 (0.5 μM CYP enzyme, 50 mM Tris, pH 7.4). Rates are reported as mean ± S.D. ($n \geq 3$) and given in nmol.nmol-CYP^{-1}.min^{-1}. The leak rate of the enzyme in the absence of substrate was 9.0 nmol.nmol-CYP^{-1}.min^{-1}. The data is reported as measured and has not been corrected for the leak rate.

described by Dawson and co-workers and classified as "normal".[29] Despite the greater shift in the $\Delta\lambda_{max}$ and peak-to-trough absorbance change with 4-(pyridin-3-yl)benzoic acid, it bound with a lower affinity (2.3 ± 0.1 versus 1.0 ± 0.1 μM, Table 1 and Figure S2).

Optical Spectroelectrochemistry

The optical spectra of ferric and ferrous CYP199A4 varied when different substrates were added presumably due to a different ligand substitution pattern or environment at the distal side of the iron. Spectroelectrochemistry (using cobalt complex mediators, Figure S3) enabled the determination of the $Fe^{III/II}$ redox potentials at pH 7.4 (Figure 3, Figure S4). The experiments also showed that the redox processes and coupled ligand substitution reactions were chemically reversible. This indicates that the oxidized and reduced forms, whether bound to substrate or not, revert to their preferred five- or six-coordinate form upon oxidation or reduction and that these ligand exchange reactions are fast on the timescale of the experiment i.e. not rate limiting.

In the absence of substrate, the redox potential of CYP199A4 was −438 mV vs NHE. This is in good agreement with the redox potential previously reported for the closely related CYP199A2 enzyme using organic mediators (−431 mV).[46, 51] When the redox potential of CYP199A4 was measured using this alternative set of mediators the redox potential was determined to be similar (Figure S5).[41] The initial spectrum of the protein, which is entirely consistent with a LS, 6-coordinate (aqua) ferric heme thiolate chromophore, changes on electrochemical reduction to the ferrous form. This results in a blue shifted Soret band (414 nm) with a decreased intensity and the α/β bands coalesce to a single peak at 548 nm (Figure 3, Table S2, Figure S4).

Shifts in the substrate-bound $Fe^{III/II}$ redox potential (E_S) relative to the substrate-free value (E′; expressed as ΔE) may provide a quantitative indication of the degree of association as shown in Scheme 1. In the presence of 4-methoxybenzoic acid a type I spectrum is seen, which is consistent with HS five-coordinate ferric heme. There is a significant positive shift in the

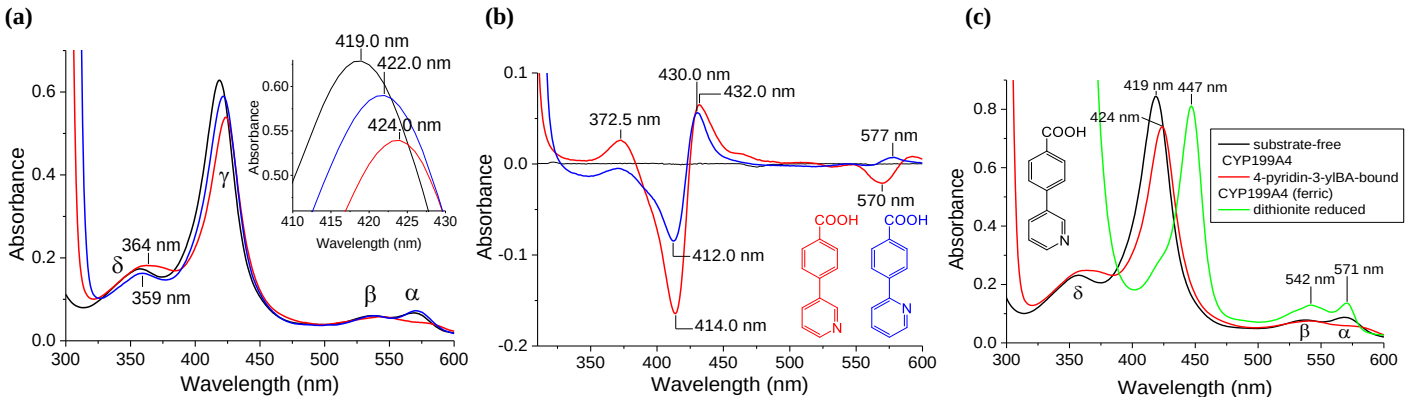

Figure 2 The overall (a) and difference (b) UV spectra of ferric CYP199A4 with 4-(pyridin-2-yl)- and 4-(pyridin-3-yl)benzoic acid and the UV spectrum (c) of ferrous CYP199A4 with 4-(pyridin-3-yl)benzoic acid. (a) The substrate-free form is shown in black and the substrate-bound form of 4-(pyridin-2-yl)benzoic acid in blue (λ_{max} 422 nm) and 4-(pyridin-3-yl)benzoic acid in red (λ_{max} 424 nm). (b) The difference spectra highlighting the UV response to substrate addition. The peak and trough for 4-(pyridin-2-yl)benzoic acid were at 430 and 412 nm, respectively while those for 4-(pyridin-3-yl)benzoic acid were at 432 and 414 nm. The concentration of the enzyme in both assays was 5.2 μM. (c) The ferric substrate-free form is shown in black and the ferric 4-(pyridin-3-yl)benzoic acid-bound form is in red (λ_{max} 424 nm). The ferrous substrate-bound form is in green (λ_{max} 447 nm).

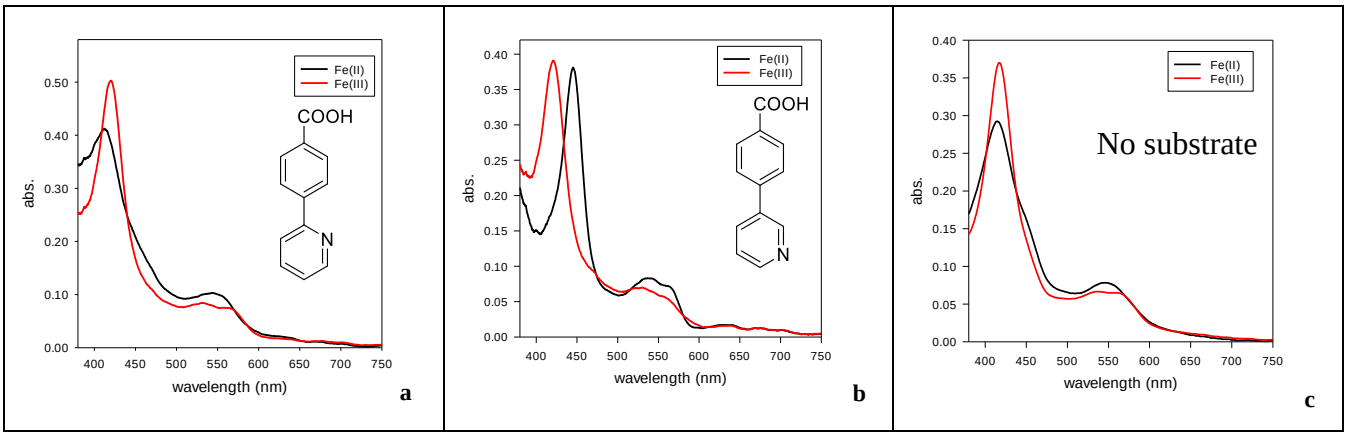

Figure 3 Calculated spectra of the ferric and ferrous forms of CYP199A4 in the presence of different substrates (all at 1 mM concentration) from the spectroelectrochemistry experiments. The substrate-free spectra are also shown for comparison (c). (a) 4-(pyridin-2-yl)benzoic acid and (b) 4-(pyridin-3-yl)benzoic acid. The spectrum for 4-methoxybenzoic acid is provided in the supporting information (Figure S4).

$Fe^{III/II}$ redox potentials in this case; ΔE = +250 mV for 4-methoxybenzoic acid (Table 1, Figure S4). This positive shift in redox potential is not unusual and has been linked to the extent of the displacement of the aqua ligand and associated outer sphere water molecules from the ferric heme, which typically favors reduction.[4, 5, 46] The redox potential of 4-methoxybenzoic acid-bound CYP199A4 was also measured at –218 ± 3 mV using a different set of mediators (Figure S5). The reduction of CYP199A4 with 4-methoxybenzoic acid bound resulted in a shift of the Soret band to ~414 nm and a merging of the α- and β-bands consistent with those of the ferrous form of CYP199A4 and other P450s.[25, 63]

Scheme 1 The substrate association constants in each oxidation state. Shifts in the substrate-bound $Fe^{III/II}$ redox potential (E_S) relative to the substrate-free value (E′) are expressed as ΔE in mV. If ΔE > 0 this reflects substrate binding effects that either stabilize the ferrous heme more than the ferric heme or destabilize the ferric heme more so than the ferrous heme relative to the substrate-free form. For ligands that coordinate to Fe in both oxidation states, the sign and value of ΔE reflects preference of a particular ligand for either Fe^{II} or Fe^{III}.

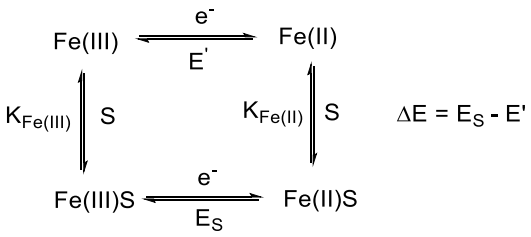

$$\frac{\Delta E}{59} = \log K_{Fe(II)} - \log K_{Fe(III)}$$

Reduction of CYP199A4 after 4-(pyridin-2-yl)benzoic acid addition resulted in a ferrous form that is indistinguishable from the spectrum of this form of the substrate-free enzyme (Figure 3a). The redox potential shifts negatively (ΔE = -34 mV) relative to the substrate-free form. Electrochemical reduction of CYP199A4 bound with the isomer 4-(pyridin-3-yl)benzoic acid brings about a profound modification in the ferrous spectra with the Soret band shifting to 447 nm and other changes in the α-/β- band region (Figure 3, Table S1 and S2). This ferrous CYP199A4 spectrum is markedly different to all others seen in this work and is consistent with reports of ferrous forms of P450s which contain a Fe-N bond at the distal coordination site.[20, 62, 64] The redox potential was –321 mV, a shift of +117 mV with respect to the substrate-free enzyme. Therefore binding of the 4-(pyridin-2-yl) isomer stabilizes the ferric form of the enzyme (or destabilizes the ferrous form) whereas 4-(pyridin-3-yl)benzoic acid has the opposite effect.

We also chemically reduced the heme in the presence of the substrates with dithionite to confirm that these spectra are consistent with the electrochemically reduced forms (Figure 1 and Figure S6). In all but one case, the spectral changes observed were consistent with those reported for the spectroelectrochemistry (Table S1 and S2). When these experiments were performed with CYP199A4 and 4-(pyridin-2-yl)benzoic acid there was little change in the spectrum with the Soret band remaining at 422 nm suggesting that reduction of this species with dithionite did not occur (Figure S6). To ascertain if binding of this substrate was preventing heme reduction the assays were repeated by adding the dithionite reducing agent before the substrate. In these experiments, the Soret band of the ferrous form shifted from 417 nm to 419 nm on addition of 4-(pyridin-2-yl)benzoic acid. Control experiments were also performed using imidazole and pyridine as ligands (Figure S7 and S8).

Substrate turnovers

In line with the type II inhibitory spin state shifts observed with both pyridinyl benzoic acids, no products were detected from enzyme catalyzed turnover. Neither substrate induced rapid NADH oxidation during these turnover assays, which is a measure of the rate of throughput in the catalytic cycle. With 4-(pyridin-2-yl)benzoic acid NADH consumption was similar to the leak rate of the system in the absence of substrate (Table 1). While NADH consumption with 4-(pyridin-3-yl)benzoic acid was faster it was still significantly slower than that seen with 4-methoxybenzoic acid and the other substrates which induced a type I spectrum upon binding (Table 1). Importantly the rate of NADH oxidation by the CYP199A4 system in the presence of all these substrates is entirely consistent with the measured redox potentials (Table 1).

The redox potential of the [2Fe-2S] ferredoxin HaPux was determined to be –232 ± 15 mV (Figure S9).[41] This is consistent with previous measurements of the related [2Fe-2S] ferredoxin, Pux from *R. palustris* CGA009, of –251 mV.[46, 51] In agreement with the measured redox potentials the physiological electron transfer partners of CYP199A4 (HaPuR and HaPux) are able to reduce CYP199A4 in the presence of 4-(pyridin-3-yl)-benzoic acid. However, when 4-(pyridin-2-yl)-benzoic acid was bound to the enzyme the reduction was not detectable using the same conditions (Figure S10).

Crystal structure of the 4-(pyridin-2-yl)- and 4-(pyridin-3-yl)-benzoic acid bound forms of CYP199A4

In order to rationalize the different CYP199A4 UV-vis spectra obtained on substrate binding with 4-(pyridin-2-yl)- and 4-(pyridin-3-yl)-benzoic acids, crystal structures of the substrate-bound forms of the enzyme for each were obtained (Table S3, Figure S11, PDBs: 6U3K and 6U30, respectively). In both CYP199A4 complexes, the overall protein fold was very similar to previous structures of this enzyme (Figure S12; the r.m.s.d. was < 0.622 Å when compared to the 4-methoxybenzoic acid-bound structure). There was electron density in the substrate binding pocket that was modeled by the appropriate pyridinyl inhibitor (Figure 4). The majority of the active site amino acids and the capping chloride were also located in comparable locations to previously reported structures (Figure S13, S14 and S15). One exception was phenylalanine (F298) which shifted to accommodate the substrate in the 4-(pyridin-2-yl)benzoic acid-bound structure. The side chain of this residue occupied a position more similar to that observed in the 4-ethylthiobenzoic acid bound-CYP199A4 structure (PDB: 5U6U, Figure 4, Figure S16).[45]

Other differences are observed between the two structures (Table S4). The benzoate moiety of the 4-(pyridin-3-yl)benzoic acid structure shifts compared to the equivalent part of the molecule in the 4-(pyridin-2-yl)benzoic acid and 4-methoxybenzoic acid structures (Figure 4, Table S5, and Figure S14 and S15). This results in a small shift in the position of the water molecule that bridges the carboxylate group with R243. The pyridine ring in 4-(pyridin-3-yl)benzoic acid rotates out of the plane of the benzene ring by 40.2°, whereas in the 4-(pyridin-2-yl)benzoic acid structure this angle is 60.6° (Table S4).

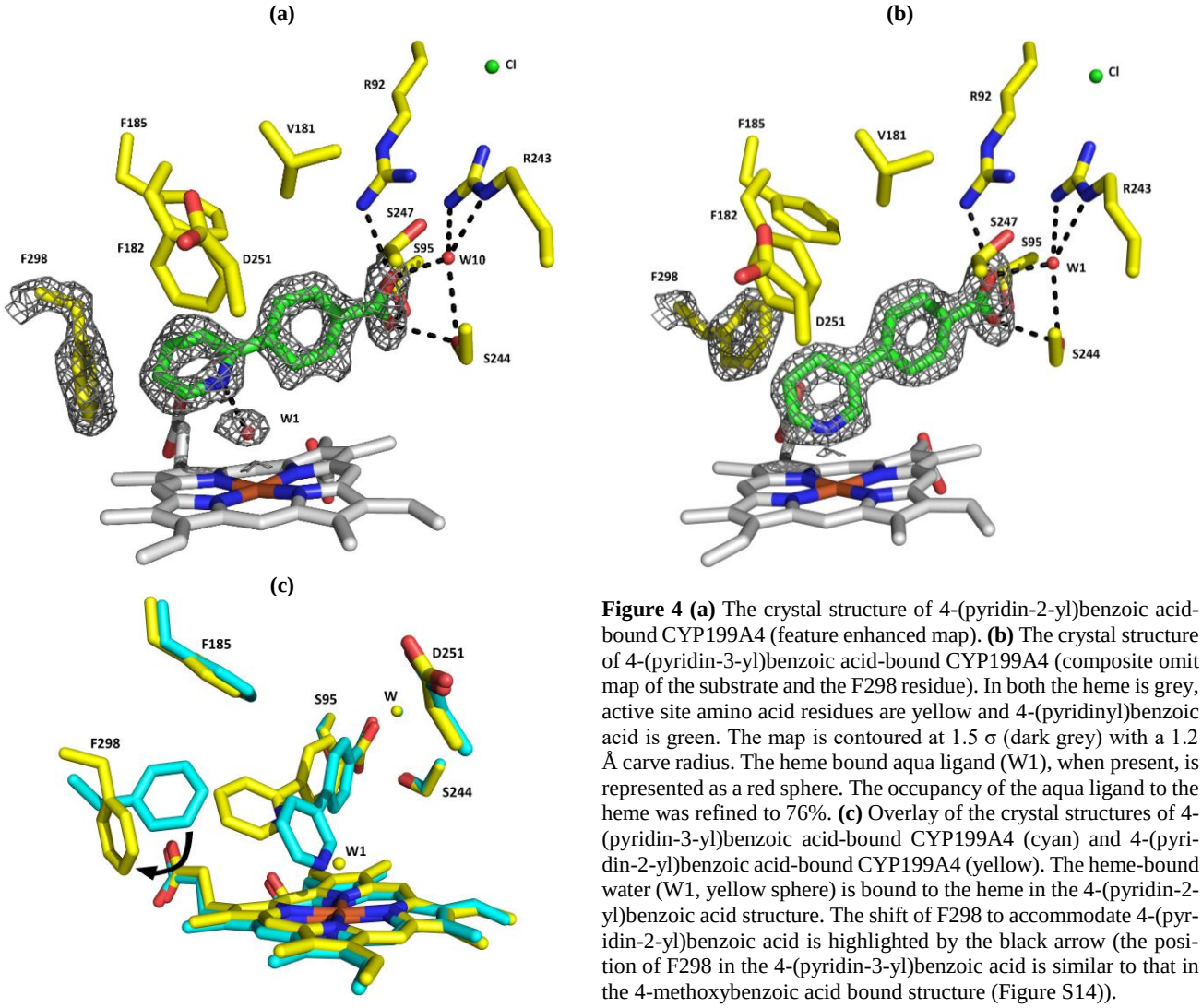

Figure 4 (a) The crystal structure of 4-(pyridin-2-yl)benzoic acid-bound CYP199A4 (feature enhanced map). **(b)** The crystal structure of 4-(pyridin-3-yl)benzoic acid-bound CYP199A4 (composite omit map of the substrate and the F298 residue). In both the heme is grey, active site amino acid residues are yellow and 4-(pyridinyl)benzoic acid is green. The map is contoured at 1.5 σ (dark grey) with a 1.2 Å carve radius. The heme bound aqua ligand (W1), when present, is represented as a red sphere. The occupancy of the aqua ligand to the heme was refined to 76%. **(c)** Overlay of the crystal structures of 4-(pyridin-3-yl)benzoic acid-bound CYP199A4 (cyan) and 4-(pyridin-2-yl)benzoic acid-bound CYP199A4 (yellow). The heme-bound water (W1, yellow sphere) is bound to the heme in the 4-(pyridin-2-yl)benzoic acid structure. The shift of F298 to accommodate 4-(pyridin-2-yl)benzoic acid is highlighted by the black arrow (the position of F298 in the 4-(pyridin-3-yl)benzoic acid is similar to that in the 4-methoxybenzoic acid bound structure (Figure S14)).

The positions of the α-carbon and β-nitrogen of 4-(pyridin-2-yl)benzoic acid-bound CYP199A4 are in a similar location to the equivalent atoms at the α- and β-positions of 4-ethyl- and 4-methoxy-benzoic acids in their crystal structures (Figure S14 and S17). The different position of the benzoic acid moiety and rotation of the pyridinyl ring of 4-(pyridin-3-yl)benzoic acid results in the latter being held closer to the heme rather than being directed towards the space vacated by the movement of the F298 residue (Figure 4, Table S5 and Figure S15). Thus, 4-(pyridin-3-yl)benzoic acid displaces the aqua ligand, allowing nitrogen to coordinate to the heme. The pyridinyl ring is not bound perpendicular to the heme plane but is at an angle of 18° to the Fe-S(Cys) axis (Figure S18). The nitrogen atom is 2.2 Å from the iron, which is closer than the equivalent *β*-carbon of 4-ethylbenzoic acid that was 3.0 Å away (Table S4, Table S6 and Figure S17). The structure of CYP199A4 with 4-(pyridin-2-yl)benzoic acid shows that the heme aqua ligand is retained (76% occupancy) and the pyridine nitrogen of the substrate interacts with ligand W1 (2.9 Å) and is 4.2 Å from the iron (Figure 4, Table S4 and Figure S14 and S18). The next closest substrate atom to the iron in this structure is C05 that is 4.4 Å away (Table S4). Importantly these structures provide a rationale for the optical spectra that are observed when these two substrates bind to CYP199A4 by clearly highlighting the different heme coordination environment.

Substrate binding in frozen-solution as determined by EPR

To further ascertain the spin-state and active site configuration of CYP199A4 after addition of 4-methoxy-, 4-(pyridin-2-yl)-, and 4-(pyridin-3-yl)-benzoic acid, as well as for substrate-free CYP199A4, CW and pulsed EPR data in frozen-solution were measured. A CW EPR spectrum provides a fingerprint for high-spin (HS) and low-spin (LS) species, as well as detecting if a substrate binds to the active site by measuring shifts in the *g*-values (especially relevant when there is no spin state change). The high-resolution pulsed EPR experiments HYSCORE and ENDOR can be used to provide further information on the proximal ligand in the LS species of CYP199A4 via measurement of small hyperfine and nuclear quadrupole interactions which are unresolved in CW EPR spectra.[28]

X-band CW EPR spectra for the set of CYP199A4 samples measured at 15 K are shown in Figure 5. Table S7 provides EPR spin Hamiltonian parameters obtained from simulation, *g*-values for each component and the percentage of HS and LS . The full set of spectra and the simulations are provided in the Supplementary Information (Table S7 and Figure S19-S22). The presence of several LS species after the addition of 4-methoxybenzoic acid indicates the presence of multiple active site conformations or substrate binding modes.

All samples, both substrate-free and ligand bound CYP199A4, contain one or more LS species. HS components were observed only for CYP199A4 samples with 4-methoxybenzoic acid (Table S7). The HS proportion determined by CW EPR in frozen-solution is less than the proportion determined through UV-vis spectroscopy at room temperature (Table 1), as is generally observed.[28, 33, 65, 66] The observation of an increase in the signal percentage arising from LS forms has been attributed to the low temperature of the EPR experiments modifying the spin-state equilibrium. A comparison of the LS components from the 4-methoxybenzoic acid spectrum with the substrate-free spectrum shows shifts in the *g*-values, consistent with substrate binding in the active site with a high occupancy (ca. 100%). In the case of both 4-(pyridin-2-yl)- and 4-(pyridin-3-yl)-benzoic acid samples only LS species are observed, indicative of six coordinated ferric heme centers. In the 4-(pyridin-2-yl)benzoic acid sample a single species was detected and the shift in all three *g*-values is very small (Figure 5, Table S7). This suggests that the substrate binds to CYP199A4 but does not displace the resting state aqua ligand in agreement with the crystal structure.[33, 35]

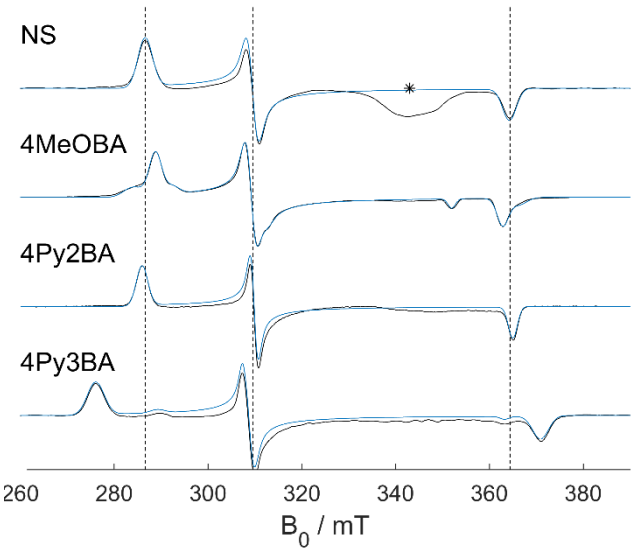

Figure 5 X-band (9.7590 GHz) CW EPR spectra recorded at 15 K showing only the low-spin field region. Spectra are from substrate-free CYP199A4 (NS) and after addition of 4-methoxybenzoic acid (4MeOBA), 4-(pyridin-2-yl)benzoic acid (4Py2BA), and 4-(pyridin-3-yl)benzoic acid (4Py3BA). Experimental trace – black. Simulation – blue, which is the sum of all EPR components (see Table S7). Figures S19-S22 show the full spectrum including any high-spin signals and the simulation for each component. A background resonator signal is marked with '*'.

In the case of 4-(pyridin-3-yl)-benzoic acid all three *g*-values of the major component shift, with large g_x and g_z changes, which supports coordination of the pyridinyl nitrogen of the substrate to the ferric paramagnetic center (Figure 6).[29] However, to definitively determine the proximal ligand on the basis of the *g*-value shifts alone carries uncertainty, and thus we sought to identify the proximal ligand using high-resolution pulsed EPR methods.

X-band HYSCORE was used to measure small ^{1}H and ^{14}N electron-nuclear couplings which are not resolved in the CW EPR data. The ^{1}H region of these spectra enable an aqua ligand to be identified through the magnitude of the dipolar part of the proton hyperfine interaction.[67] The substrate-free CYP199A4 spectrum (Figure 6a) displays typical ^{1}H hyperfine coupling ridges characteristic of water axially coordinated to the ferric heme paramagnetic center of the P450 enzyme.[67,68] HYSCORE spectra collected on samples with 4-(pyridin-2-yl)-benzoic acid (Figure 6b) display characteristic water ^{1}H signals allowing the proximal aqua ligand to be unambiguously identified.

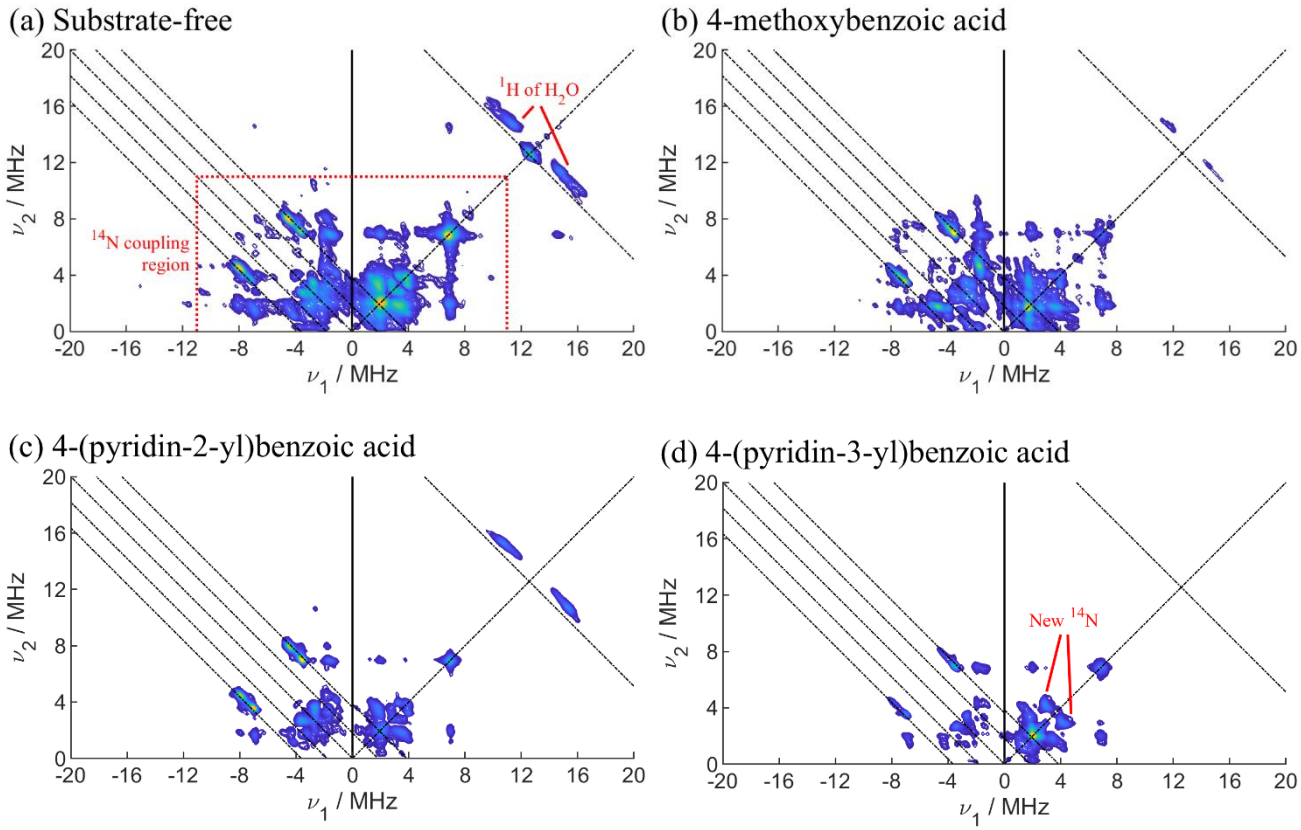

Figure 6 X-band (~9.738 GHz) HYSCORE spectra measured at 12.5 K from substrate-free CYP199A4 (a) and after addition of (b) 4-methoxybenzoic acid, (c) 4-(pyridin-2-yl)benzoic acid and (d) 4-(pyridin-3-yl)benzoic acid. In (a) and (c) anisotropic proton hyperfine coupling ridges characteristic of directly-coordinated water molecules are visible in the weak coupling quadrant (+,+).In the 4-(pyridin-3-yl)benzoic acid sample (d) water ^{1}H couplings are absent, indicating the ligand coordinates directly to the Fe^{III} ion. With 4-methoxybenzoic acid (b) the intensity of these signals is very weak indicating low water occupancy. In all spectra peaks at frequencies < 9 MHz in both the strong (–,+) and weak (+,+) coupling quadrants are characteristic of coordinated heme pyrrole nitrogens; these signals change slightly with different ligands and in the sample with 4-(pyridin-3-yl)benzoic acid the appearance of new cross-peaks is consistent with direct coordination by nitrogen.

The HYSCORE spectrum from the LS species of the 4-methoxybenzoic acid-bound CYP199A4 sample (Figure 6b) only displays signals with very low intensities that are characteristic of an aqua ligand, indicating that this substrate largely displaces the water coordinated to iron in the active site of substrate-free enzyme. Similarly, the CYP199A4 with 4-(pyridin-3-yl)benzoic acid sample shows a HYSCORE spectrum (Figure 6d) without characteristic proton ridges from an aqua ligand, in agreement with the distal ligand in this case being the nitrogen of the 4-(pyridin-3-yl)benzoic acid substrate (Figure 6d). Further information on ligand coordination with this substrate was obtained by the appearance of new ^{14}N HYSCORE signals in additional to the normal peaks from the ^{14}N pyrrole nitrogens.[37] This can be seen by comparison of HYSCORE spectra from the substrate-free to the 4-(pyridin-3-yl)benzoic acid bound CYP199A4 samples where the new ^{14}N peaks are clearly identified in the latter. To further confirm coordination of the 4-(pyridin-3-yl)benzoic acid ligand X-band Mims ENDOR spectra in the ^{14}N frequency range were collected (Figure S23). The ENDOR spectra of all the substrates except 4-(pyridin-3-yl)benzoic acid exhibit characteristic ^{14}N pyrrole signals that are all very similar and thus demonstrate that the electronic structure of the LS forms of these species is not significantly altered. Conversely, the 4-(pyridin-3-yl)benzoic acid sample shows additional intense signals from a strongly coupled ^{14}N nucleus which confirms binding of the pyridin-3-yl nitrogen to the ferric iron of the heme.

The above EPR data show that all substrates investigated bind (either noncovalently or through coordination) to ferric CYP199A4. A significant proportion of the sample is the aqua complex with 4-(pyridin-2-yl)-benzoic acid, whereas 4-methoxybenzoic acid displaces the aqua ligand to give a five coordinate HS state (with potentially some binding from another oxygen donor in the frozen solution EPR resulting in a six coordinate LS complex). Addition of 4-(pyridin-3-yl)benzoic acid to CYP199A4 leads to ligand substitution of aqua ligand by the pyridinyl N-donor.

Comparison of the CYP199A4 substrate binding modes

A comparison of the spectroelectrochemical and biochemical data for CYP199A4 and the different substrates along with the now available crystal structure of each enables detailed analysis of the heme binding environment and the properties of the enzyme. We can consider three different substrate binding scenarios; the first, archetypal type I binding generates a 5-coordinate

heme as observed with 4-methoxybenzoic acid and other substrates such as 4-ethylbenzoic acid.[7, 43] 4-(Pyridin-2-yl)benzoic acid provides an example of a type II substrate which does not fully displace the 6th aqua ligand from the iron. In this instance reduction of the iron leads to dissociation of the aqua ligand. Finally, 4-(pyridin-3-yl)benzoic acid forms a type II 6-coordinate ferric P450 complex with nitrogen coordination at the distal position. Reduction results in a 6-coordinate ferrous species maintaining the Fe-N bond. All of these different coordination states and environments around the heme, including the bond lengths as well as the angle of approach of the donor ligand, have an impact on the $Fe^{III/II}$ redox potential.

Comparison of the iron coordination environment of the ferric species in each of the crystal structures also highlights other differences. As is typical of substrates which generate a 5-coordinate HS substrate-bound ferric P450, the CYP199A4 iron is drawn toward the axial Cys ligand and sits below the plane of the porphyrin ring and its coordinating nitrogen donors (by 0.20 - 0.31 Å, Figure S24, Table S8). This is in line with previously reported crystal structures of this and other enzymes.[7, 43, 45, 69, 70] Both of the 6-coordinate species have the iron more in the plane of the porphyrin ring (Figure S24, Table S8). The iron in those structure with a nitrogen donor at the distal coordination site moves further into the plane (0.05 Å below the pyrrole nitrogens) than that with water (0.13 Å). The length of the iron-cysteinate sulfur and the iron-porphyrin ring nitrogens were also measured (Table S9 and S10). Only minor changes were observed in the latter. For the 6-coordinate type II ligand the Fe-S bond length was marginally shorter than in the 5-coordinate heme structures (2.29 - 2.30 Å versus 2.34 - 2.40 Å, Table S9). These changes would also be expected to contribute to the varying redox potential of CYP199A4 with the different ligands.

Discussion

The altered type II spectra observed between the two pyridine based inhibitor molecules may be rationalized by the different coordination modes of binding observed in the X-ray crystal structures. Others have reported that nitrogen donor ligands which are coordinated to the iron and those which bind non-covalently with the iron-bound aqua ligand are difficult to distinguish based on UV-Vis spectra.[23, 34] In the CYP199A4 system, coordination of nitrogen to the heme induced a greater absolute shift in the wavelength of the Soret band. The changes in the optical spectra of 4-(pyridin-3-yl)benzoic acid reflect those of the "normal" (N-coordination) nitrogen donors to P450cam described by Dawson and co-workers in experiments used to help identify the sixth ligand of P450cam (CYP101A1). In contrast, the optical spectrum of the 4-(pyridin-2-yl)benzoic acid-CYP199A4 complex shows clear differences and could be described as an "abnormal" nitrogen donor. One feature of the optical spectrum of 4-(pyridin-2-yl)benzoic acid-bound CYP199A4 is that it has an α-band which is more intense than the β-band. This is characteristic of complexes of P450cam with oxygen donor ligands and those which do not displace the water. This work highlights that closer inspection of the α-, β-, and δ- regions in the absolute and difference spectra may highlight different binding modes more reliably. One potential reason for this situation being more complex in other systems may be that the molecules may bind in multiple conformations which complicates analysis. This could arise if the small molecule inhibitors do not resemble the physiological substrates of the P450s or if the enzyme has evolved to bind a broad range of substrates and is conformationally flexible.

Electrochemical or chemical reduction of the CYP199A4 ferric substrate-bound complexes to the ferrous form provided further evidence for nitrogen coordination with 4-(pyridin-3-yl)benzoic acid but not the pyridin-2-yl isomer. EPR measurements reveal that the situation in solution, albeit at low temperatures, was consistent with that observed in the UV-Vis spectra and the X-ray crystal structures. Importantly EPR evidence was observed for N-coordination by 4-(pyridin-3-yl)benzoic acid but not for 4-(pyridin-2-yl)benzoic acid. For the latter substrate there was strong evidence from HYSCORE of an aqua ligand in agreement with the X-ray crystal structure.

Jones *et al*. have previously observed that type II ligands, which form axial Fe-N bonds, bind with substantially higher affinity than analogues that bind in a type I fashion.[18, 19] They utilized quinoline-4-carboxamide analogues incorporating a pyridine moiety in which the location of the nitrogen was varied.[18] Those compounds with the nitrogen in the *para* position were capable of forming Fe-N bonds, but not those with the nitrogen in the *ortho* or *meta* positions.[18] Analogues which formed Fe-N bonds with the heme were found to bind with up to 4200-fold greater affinity than those which did not coordinate to the iron.[18] Despite forming an Fe-N bond with the heme, 4-(pyridin-3-yl)benzoic acid displays lower affinity for CYP199A4 than 4-(pyridin-2-yl)benzoic acid (K_d = 2.3 μM *vs.* 1.0 μM). The crystal structures reveal that the orientation of 4-(pyridin-3-yl)benzoic acid in the active site differs substantially from the orientation of 4-(pyridin-2-yl)benzoic acid and other substrates such as 4-methoxybenzoic acid. It therefore seems that in order for 4-(pyridin-3-yl)benzoic acid to coordinate to the iron, it must adopt a strained and less favorable orientation in the active site which must counteract the gain in affinity resulting from formation of the Fe-N bond.

The aromatic heterocyclic ring was not perpendicular to the heme in any of the CYP199A4 complexes. Ideally the nitrogen containing ring would be perpendicular to the heme (Table S4, Figure S18 and S25).[35, 71, 24] This and the longer bond could indicate weaker than expected Fe-N bonds which are compensated for by other ligand binding interactions. The attachment of the pyridinyl ring to a benzoic acid substituent, and the requirement of other interactions in the active site presumably prevents optimal Fe-N bond formation at the heme.

CW EPR provided evidence for conformational heterogeneity in substrate-bound forms of CYP199A4, at least at low temperature. This is consistent with reports of other P450 enzymes which show this type of behavior when investigated via EPR and other spectroscopies. This could arise from open and closed forms of the P450, as observed with P450cam and others,[47, 72-74] or from changes in the location of the active site residues such as F298 of CYP199A4, which has been shown to move in various X-ray crystal structures depending on the size of the substrate. As with other P450s, a mixture of high-spin and low-spin species were observed by EPR and the percentage of low-spin species is higher in frozen solution.

The positive shift in the redox potentials with 4-methoxybenzoic acid is in agreement with those reported previously for type I substrates. The relationship between the magnitude of the redox potential shift, the measured spin state, the extent of aqua ligand occupancy and the rate of turnover of the catalytic cycle are as expected. It is often stated that coordination of a stronger

nitrogen donor should lower the redox potential and this is purported to be one of the major reasons why these molecules inhibit P450 activity. However, there are only a few reported examples of such measurements in the literature.[20, 75] The redox potential of CYP199A4 with 4-(pyridin-3-yl)benzoic acid, in which the ligand remains bound on reduction to give a 6-coordinate ferrous heme, resulted in a significant positive shift in the $Fe^{III/II}$ redox potential. Therefore, addition of this substrate results in a stabilization of the ferrous form of the enzyme relative to the ferric when compared to the substrate-free form. The mechanism of CYP199A4 inhibition with 4-(pyridin-3-yl)benzoic acid therefore seems not to be directly related to the effect on the $Fe^{III/II}$ redox potential and would be due to competitive inhibition of substrate or dioxygen binding. 4-(Pyridin-2-yl)-benzoic acid was the only ligand that lowered the redox potential of CYP199A4 compared to the substrate-free form. This shift was relatively small which is in agreement with the presence of the aqua ligand in the six-coordinate LS form. Reduction and resulting removal of the 6^{th} distal ligand appears to be more difficult than in the substrate-free form. Intriguingly the results suggest that this type of heme coordination environment could result in better P450 inhibitors than those coordinated through a nitrogen donor. Although the factors that control the redox potentials of cytochrome P450 enzymes are complex it is tempting to speculate that the ease of reduction of ferric CYP199A4 observed here could be related to the strength of the distal ligand bonding. Stronger coordination of an aqua ligand makes the system more difficult to reduce in the case of 4-(pyridin-2-yl)benzoic acid. Nitrogen-donor coordination may not always result in a higher redox potential perhaps if, as is observed here with an aromatic heterocyclic substrate, the ligand cannot bind in an optimal position to the iron.

Conclusion

Application of multiple spectroscopic techniques and measurements are required to fully understand substrate binding in different cytochrome P450 monooxygenases. Here we show that detailed analysis of the optical spectra (using readily available UV-vis spectroscopy) can differentiate between nitrogen ligand coordination and noncovalent binding through a bridging aqua ligand for type II substrates. These observations were confirmed by X-ray crystallography and EPR spectroscopy. The spectra measured here for the ferric and ferrous forms, as well as those previously published for the normal and abnormal binding modes of P450cam, are valuable in assessing if other measured optical difference spectra could arise from these different type II and type I binding modes or populations of them. The redox potentials highlight that nitrogen ligand coordination may not always result in the best P450 inhibitors. The crystal structures and EPR identified other differences in the heme environment such as ligand coordination and the location of the iron relative to the porphyrin ring and coordinating cysteine, which could have an impact on the redox potential and catalytic activity of P450 enzymes with different substrates. Measurement of the UV spectrum and redox potential are both critically important when assessing the binding modes and mechanism of action of drug molecule inhibitors with microbial and membrane-bound eukaryotic P450 enzymes.

ASSOCIATED CONTENT

Supporting Information. The Supporting Information is available free of charge via the Internet at http://pubs.acs.org.

This consists of additional experimental details, UV-vis spectroscopy, spectroelectrochemistry and mediator details, crystal structure data, EPR spectroscopy and comparative structural information.

ACCESSION CODES

CYP199A4 Uniprot: Q2IU02

HaPux Uniprot: Q2IU01

HaPuR Uniprot: Q2ITV9

AUTHOR INFORMATION

Corresponding Authors

* stephen.bell@adelaide.edu.au
* jeffrey.harmer@cai.uq.edu.au
* j.devoss@uq.edu.au
* p.bernhardt@uq.edu.au

Author Contributions

All authors have given approval to the final version of the manuscript. ⊥ The authors MNP, JSH and TC contributed equally.

ACKNOWLEDGMENT

This work was in part supported by ARC grant DP140103229 (to JJDV and SGB). SGB and JRH acknowledge the ARC for Future Fellowships (FT140100355 and FT120100421, respectively). The authors also acknowledge the award of an Australian Government Research Training Program Scholarships (PhD to TC and MPhil to MNP) and a University of Queensland PhD Scholarship to JSH. JAY was supported by NSERC, Canada, and The Rhodes Trust. We would like to thank the scientists at MX1 and MX2 beamline for help with data collection. We acknowledge ANSTO for financial support and in providing the facility used in this work.

REFERENCES

[1] Greule, A., Stok, J. E., De Voss, J. J., and Cryle, M. J. (2018) Unrivalled diversity: the many roles and reactions of bacterial cytochromes P450 in secondary metabolism, *Nat. Prod. Rep. 35*, 757-791.

[2] Guengerich, F. P., and Munro, A. W. (2013) Unusual cytochrome p450 enzymes and reactions, *J. Biol. Chem. 288*, 17065-17073.

[3] Rendic, S., and Guengerich, F. P. (2012) Contributions of human enzymes in carcinogen metabolism, *Chem. Res. Toxicol. 25*, 1316-1383.

[4] Fisher, M. T., and Sligar, S. G. (1985) Control of heme protein redox potential and reduction rate: linear free energy relation between potential and ferric spin state equilibrium, *J. Am. Chem. Soc. 107*, 5018-5019.

[5] Sligar, S. G., and Gunsalus, I. C. (1976) A thermodynamic model of regulation: modulation of redox equilibria in camphor monoxygenase, *Proc. Natl. Acad. Sci. U. S. A. 73*, 1078-1082.

[6] Honeychurch, M. J., Hill, A. O., and Wong, L. L. (1999) The thermodynamics and kinetics of electron transfer in the cytochrome P450cam enzyme system, *FEBS Lett. 451*, 351-353.

[7] Bell, S. G., Zhou, R., Yang, W., Tan, A. B., Gentleman, A. S., Wong, L. L., and Zhou, W. (2012) Investigation of the substrate range of CYP199A4: modification of the partition between hydroxylation and desaturation activities by substrate and protein engineering, *Chemistry 18*, 16677-16688.

[8] Chao, R. R., De Voss, J. J., and Bell, S. G. (2016) The efficient and selective catalytic oxidation of para-substituted cinnamic acid derivatives by the cytochrome P450 monooxygenase, CYP199A4, *RSC Adv. 6*, 55286-55297.

[9] Coleman, T., Chao, R. R., De Voss, J., and Bell, S. G. (2016) The importance of the benzoic acid carboxylate moiety for substrate recognition by CYP199A4 from *Rhodopseudomonas palustris* HaA2, *Biochim. Biophys. Acta Proteins Proteomics 1864*, 667-675.

[10] Ogliaro, F., de Visser, S. P., Cohen, S., Sharma, P. K., and Shaik, S. (2002) Searching for the second oxidant in the catalytic cycle of cytochrome P450: a theoretical investigation of the iron(III)-hydroperoxo species and its epoxidation pathways, *J. Am. Chem. Soc. 124*, 2806-2817.

[11] Rittle, J., and Green, M. T. (2010) Cytochrome P450 compound I: capture, characterization, and C-H bond activation kinetics, *Science 330*, 933-937.

[12] Sharma, P. K., De Visser, S. P., and Shaik, S. (2003) Can a single oxidant with two spin states masquerade as two different oxidants? A study of the sulfoxidation mechanism by cytochrome p450, *J. Am. Chem. Soc. 125*, 8698-8699.

[13] Meunier, B., de Visser, S. P., and Shaik, S. (2004) Mechanism of oxidation reactions catalyzed by cytochrome p450 enzymes, *Chem. Rev. 104*, 3947-3980.

[14] Shaik, S., Cohen, S., Wang, Y., Chen, H., Kumar, D., and Thiel, W. (2010) P450 enzymes: their structure, reactivity, and selectivity-modeled by QM/MM calculations, *Chem. Rev. 110*, 949-1017.

[15] Ortiz de Montellano, P. R. (2010) Hydrocarbon hydroxylation by cytochrome P450 enzymes, *Chem. Rev. 110*, 932-948.

[16] Groves, J. T., and McClusky, G. A. (1976) Aliphatic hydroxylation via oxygen rebound - oxygen-transfer catalyzed by iron, *J. Am. Chem. Soc. 98*, 859-861.

[17] Sarkar, M. R., Houston, S. D., Savage, G. P., Williams, C. M., Krenske, E. H., Bell, S. G., and De Voss, J. J. (2019) Rearrangement-Free Hydroxylation of Methylcubanes by a Cytochrome P450: The Case for Dynamical Coupling of C–H Abstraction and Rebound, *J. Am. Chem. Soc.*

[18] Peng, C.-C., Cape, J. L., Rushmore, T., Crouch, G. J., and Jones, J. P. (2008) Cytochrome P450 2C9 type II binding studies on quinoline-4-carboxamide analogues, *J. Med. Chem. 51*, 8000-8011.

[19] Peng, C.-C., Pearson, J. T., Rock, D. A., Joswig-Jones, C. A., and Jones, J. P. (2010) The effects of type II binding on metabolic stability and binding affinity in cytochrome P450 CYP3A4, *Arch. Biochem. Biophys. 497*, 68-81.

[20] Sevrioukova, I. F., and Poulos, T. L. (2013) Pyridine-substituted desoxyritonavir is a more potent inhibitor of cytochrome P450 3A4 than ritonavir, *J. Med. Chem. 56*, 3733-3741.

[21] Lepesheva, G. I., Friggeri, L., and Waterman, M. R. (2018) CYP51 as drug targets for fungi and protozoan parasites: past, present and future, *Parasitology 145*, 1820-1836.

[22] Ortiz de Montellano, P. R., (Ed.) (2015) *Cytochrome P450: Structure, Mechanism, and Biochemistry* 4th ed., Springer International Publishing, Switzerland.

[23] Conner, K. P., Vennam, P., Woods, C. M., Krzyaniak, M. D., Bowman, M. K., and Atkins, W. M. (2012) 1,2,3-Triazole-heme interactions in cytochrome P450: functionally competent triazole-water-heme complexes, *Biochemistry 51*, 6441-6457.

[24] Locuson, C. W., Hutzler, J. M., and Tracy, T. S. (2007) Visible spectra of type II cytochrome P450-drug complexes: evidence that "incomplete" heme coordination is common, *Drug Metab. Dispos. 35*, 614-622.

[25] Luthra, A., Denisov, I. G., and Sligar, S. G. (2011) Spectroscopic features of cytochrome P450 reaction intermediates, *Arch. Biochem. Biophys. 507*, 26-35.

[26] Mak, P. J., and Denisov, I. G. (2018) Spectroscopic studies of the cytochrome P450 reaction mechanisms, *Biochim. Biophys. Acta Proteins Proteom. 1866*, 178-204.

[27] Jefcoate, C. R. (1978) Measurement of substrate and inhibitor binding to microsomal cytochrome P-450 by optical-difference spectroscopy, *Methods Enzymol. 52*, 258-279.

[28] Harbort, J. S., De Voss, J. J., Stok, J. E., Bell, S. G., and Harmer, J. R. (2017) CW and pulse EPR of Cytochrome P450 to determine structure and function, In *Future Directions in Metalloprotein and Metalloenzyme Research* (Hanson, G., and Berliner, L., Eds.), pp 103-142, Springer International Publishing, Cham.

[29] Dawson, J. H., Andersson, L. A., and Sono, M. (1982) Spectroscopic investigations of ferric cytochrome P-450-CAM ligand complexes. Identification of the ligand trans to cysteinate in the native enzyme, *J. Biol. Chem. 257*, 3606-3617.

[30] Sono, M., Andersson, L. A., and Dawson, J. H. (1982) Sulfur donor ligand binding to ferric cytochrome P-450-CAM and myoglobin. Ultraviolet-visible absorption, magnetic circular dichroism, and electron paramagnetic resonance spectroscopic investigation of the complexes, *J. Biol. Chem. 257*, 8308-8320.

[31] Andersson, L. A., and Dawson, J. H. (1984) The influence of oxygen donor ligation on the spectroscopic properties of ferric cytochrome P-450: ester, ether and ketone co-ordination to the haem iron, *Xenobiotica 14*, 49-61.

[32] Cruce, A. A., Lockart, M., and Bowman, M. K. (2015) Pulsed EPR in the study of drug binding in Cytochrome P450 and NOS, *Methods Enzymol. 563*, 311-340.

[33] Lockart, M. M., Rodriguez, C. A., Atkins, W. M., and Bowman, M. K. (2018) CW EPR parameters reveal cytochrome P450 ligand binding modes, *J. Inorg. Biochem. 183*, 157-164.

[34] Conner, K. P., Cruce, A. A., Krzyaniak, M. D., Schimpf, A. M., Frank, D. J., Ortiz de Montellano, P., Atkins, W. M., and Bowman, M. K. (2015) Drug modulation of water-heme interactions in low-spin P450 complexes of CYP2C9d and CYP125A1, *Biochemistry 54*, 1198-1207.

[35] Seward, H. E., Roujeinikova, A., McLean, K. J., Munro, A. W., and Leys, D. (2006) Crystal structure of the *Mycobacterium tuberculosis* P450 CYP121-fluconazole complex reveals new azole drug-P450 binding mode, *J. Biol. Chem. 281*, 39437-39443.

[36] Conner, K. P., Woods, C. M., and Atkins, W. M. (2011) Interactions of cytochrome P450s with their ligands, *Arch. Biochem. Biophys. 507*, 56-65.

[37] Maurelli, S., Chiesa, M., Giamello, E., Di Nardo, G., Ferrero, V. E., Gilardi, G., and Van Doorslaer, S. (2011) Direct spectroscopic evidence for binding of anastrozole to the iron heme of human aromatase. Peering into the mechanism of aromatase inhibition, *Chem. Commun. 47*, 10737-10739.

[38] Chuo, S. W., Liou, S. H., Wang, L. P., Britt, R. D., Poulos, T. L., Sevrioukova, I. F., and Goodin, D. B. (2019) Conformational Response of N-Terminally Truncated Cytochrome P450 3A4 to Ligand Binding in Solution, *Biochemistry 58*, 3903-3910.

[39] Davydov, R., Im, S., Shanmugam, M., Gunderson, W. A., Pearl, N. M., Hoffman, B. M., and Waskell, L. (2016) Role of the Proximal Cysteine Hydrogen Bonding Interaction in Cytochrome P450 2B4 Studied by Cryoreduction, Electron Paramagnetic Resonance, and Electron-Nuclear Double Resonance Spectroscopy, *Biochemistry 55*, 869-883.

[40] Hayakawa, S., Matsumura, H., Nakamura, N., Yohda, M., and Ohno, H. (2013) Spectroscopic characterization of the acid-alkaline transition of a thermophilic cytochrome P450, *FEBS Lett. 587*, 94-97.

[41] Kuznetsov, V. Y., Blair, E., Farmer, P. J., Poulos, T. L., Pifferitti, A., and Sevrioukova, I. F. (2005) The putidaredoxin reductase-putidaredoxin electron transfer complex: theoretical and experimental studies, *J. Biol. Chem. 280*, 16135-16142.

[42] Bell, S. G., Tan, A. B., Johnson, E. O., and Wong, L. L. (2010) Selective oxidative demethylation of veratric acid to vanillic acid by CYP199A4 from *Rhodopseudomonas palustris* HaA2, *Mol. Biosyst. 6*, 206-214.

[43] Bell, S. G., Yang, W., Tan, A. B., Zhou, R., Johnson, E. O., Zhang, A., Zhou, W., Rao, Z., and Wong, L. L. (2012) The crystal structures of 4-methoxybenzoate bound CYP199A2 and CYP199A4: structural changes on substrate binding and the identification of an anion binding site, *Dalton Trans. 41*, 8703-8714.

[44] Coleman, T., Chao, R. R., Bruning, J. B., De Voss, J., and Bell, S. G. (2015) CYP199A4 catalyses the efficient demethylation and demethenylation of para-substituted benzoic acid derivatives, *RSC Adv. 5*, 52007 - 52018.

[45] Coleman, T., Wong, S. H., Podgorski, M. N., Bruning, J. B., De Voss, J. J., and Bell, S. G. (2018) Cytochrome P450 CYP199A4 from *Rhodopseudomonas palustris* catalyzes heteroatom dealkylations, sulfoxidation, and amide and cyclic hemiacetal formation, *ACS Catal. 8*, 5915-5927.

[46] Bell, S. G., McMillan, J. H., Yorke, J. A., Kavanagh, E., Johnson, E. O., and Wong, L. L. (2012) Tailoring an alien ferredoxin to support native-like P450 monooxygenase activity, *Chem. Commun. 48*, 11692-11694.

[47] Bell, S. G., Xu, F., Forward, I., Bartlam, M., Rao, Z., and Wong, L.-L. (2008) Crystal structure of CYP199A2, a para-substituted benzoic acid oxidizing cytochrome P450 from *Rhodopseudomonas palustris*, *J. Mol. Biol. 383*, 561-574.

[48] Bernhardt, P. V., Chen, K.-I., and Sharpe, P. C. (2006) Transition metal complexes as mediator-titrants in protein redox potentiometry, *J. Biol. Inorg. Chem. 11*, 930-936.

[49] He, F. M. C., and Bernhardt, P. V. (2017) Cobalt cage complexes as mediators of protein electron transfer, *J. Biol. Inorg. Chem. 22*, 775-788.

[50] King, P., and Maeder, M. (2014) Reactlab Redox, J Plus Consulting Pty Ltd, Western Australia.

[51] Yorke, J. A. (2012) Engineering cytochrome P450BM3 into a drug metabolising enzyme, Oxford University, UK.

[52] Cowieson, N. P., Aragao, D., Clift, M., Ericsson, D. J., Gee, C., Harrop, S. J., Mudie, N., Panjikar, S., Price, J. R., Riboldi-Tunnicliffe, A., Williamson, R., and Caradoc-Davies, T. (2015) MX1: a bending-magnet crystallography beamline serving both chemical and macromolecular crystallography communities at the Australian Synchrotron, *J. Synchrotron Radiat. 22*, 187-190.

[53] McPhillips, T. M., McPhillips, S. E., Chiu, H. J., Cohen, A. E., Deacon, A. M., Ellis, P. J., Garman, E., Gonzalez, A., Sauter, N. K., Phizackerley, R. P., Soltis, S. M., and Kuhn, P. (2002) Blu-Ice and the Distributed Control System: software for data acquisition and instrument control at macromolecular crystallography beamlines, *J. Synchrotron Radiat. 9*, 401-406.

[54] Battye, T. G., Kontogiannis, L., Johnson, O., Powell, H. R., and Leslie, A. G. (2011) iMOSFLM: a new graphical interface for diffraction-image processing with MOSFLM, *Acta Crystallogr. D Biol. Crystallogr. 67*, 271-281.

[55] Evans, P. R., and Murshudov, G. N. (2013) How good are my data and what is the resolution?, *Acta Crystallogr. D: Biol. Crystallogr. 67*, 1204-1214.

[56] Winn, M. D., Ballard, C. C., Cowtan, K. D., Dodson, E. J., Emsley, P., Evans, P. R., Keegan, R. M., Krissinel, E. B., Leslie, A. G., McCoy, A., McNicholas, S. J., Murshudov, G. N., Pannu, N. S., Potterton, E. A., Powell, H. R., Read, R. J., Vagin, A., and Wilson, K. S. (2011) Overview of the CCP4 suite and current developments, *Acta Crystallogr. D: Biol. Crystallogr. 67*, 235-242.

[57] McCoy, A. J., Grosse-Kunstleve, R. W., Adams, P. D., Winn, M. D., Storoni, L. C., and Read, R. J. (2007) Phaser crystallographic software, *J. Appl. Crystallogr. 40*, 658-674.

[58] Emsley, P., Lohkamp, B., Scott, W. G., and Cowtan, K. (2010) Features and development of Coot, *Acta Crystallogr. D: Biol. Crystallogr. 66*, 486-501.

[59] Adams, P. D., P. V. Afonine, G. B., V. B. Chen I. W. Davis N. Echols J. J. Headd L.-W. Hung G. J. Kapral R. W. Grosse-Kunstleve A. J. McCoy N. W. Moriarty R. Oeffner R. J. Read D. C. Richardson J. S. Richardson T. C. Terwilliger, and Zwart, P. H. (2010) PHENIX: a comprehensive Python-based system for macromolecular structure solution, *Acta Crystallogr. D: Biol. Crystallogr. 66*, 213-221.

[60] Stoll, S., and Schweiger, A. (2006) EasySpin, a comprehensive software package for spectral simulation and analysis in EPR, *J. Magn. Reson. 178*, 42-55.

[61] Hanson, G. R., Gates, K. E., Noble, C. J., Griffin, M., Mitchell, A., and Benson, S. (2004) XSophe-Sophe-XeprView®. A computer simulation software suite (v. 1.1.3) for the analysis of continuous wave EPR spectra, *J. Inorg. Biochem. 98*, 903-916.

[62] Dawson, J. H., Andersson, L. A., and Sono, M. (1983) The diverse spectroscopic properties of ferrous cytochrome P-450-CAM ligand complexes, *J. Biol. Chem. 258*, 13637-13645.

[63] Child, S. A., Naumann, E. F., Bruning, J. B., and Bell, S. G. (2018) Structural and functional characterisation of the cytochrome P450 enzyme CYP268A2 from *Mycobacterium marinum*, *Biochem. J. 475*, 705-722.

[64] Sevrioukova, I. F., and Poulos, T. L. (2010) Structure and mechanism of the complex between cytochrome P4503A4 and ritonavir, *Proc. Natl. Acad. Sci. U. S. A. 107*, 18422-18427.

[65] Gantt, S. L., Denisov, I. G., Grinkova, Y. V., and Sligar, S. G. (2009) The critical iron-oxygen intermediate in human aromatase, *Biochem. Biophys. Res. Commun. 387*, 169-173.

[66] Lipscomb, J. D. (1980) Electron paramagnetic resonance detectable states of cytochrome P-450cam, *Biochemistry 19*, 3590-3599.

[67] Goldfarb, D., Bernardo, M., Thomann, H., Kroneck, P. M. H., and Ullrich, V. (1996) Study of water binding to Low-Spin Fe(III) in Cytochrome P450 by pulsed ENDOR and four-Pulse ESEEM spectroscopies, *J. Am. Chem. Soc. 118*, 2686-2693.

[68] Thomann, H., Bernardo, M., Goldfarb, D., Kroneck, P. M. H., and Ullrich, V. (1995) Evidence for water binding to the Fe centre in Cytochrome P450cam obtained by ^{17}O electron spin echo envelope modulation Spectroscopy, *J. Am. Chem. Soc. 117*, 8243-8251.

[69] Poulos, T. L., Finzel, B. C., and Howard, A. J. (1987) High-resolution crystal structure of cytochrome P450cam, *J. Mol. Biol. 195*, 687-700.

[70] Schlichting, I., Berendzen, J., Chu, K., Stock, A. M., Maves, S. A., Benson, D. E., Sweet, R. M., Ringe, D., Petsko, G. A., and Sligar, S. G. (2000) The catalytic pathway of cytochrome p450cam at atomic resolution, *Science 287*, 1615-1622.

[71] Verras, A., Alian, A., and Ortiz de Montellano, P. R. (2006) Cytochrome P450 active site plasticity: attenuation of imidazole binding in cytochrome P450cam by an L244A mutation, *Prot. Eng. Des. Sel. 19*, 491-496.

[72] Yang, W., Bell, S. G., Wang, H., Zhou, W., Bartlam, M., Wong, L. L., and Rao, Z. (2011) The structure of CYP101D2 unveils a potential path for substrate entry into the active site, *Biochem. J. 433*, 85-93.

[73] Lee, Y. T., Glazer, E. C., Wilson, R. F., Stout, C. D., and Goodin, D. B. (2011) Three clusters of conformational states in p450cam reveal a multistep pathway for closing of the substrate access channel, *Biochemistry 50*, 693-703.

[74] Tripathi, S., Li, H., and Poulos, T. L. (2013) Structural basis for effector control and redox partner recognition in cytochrome P450, *Science 340*, 1227-1230.

[75] Pearson, J., Dahal, U. P., Rock, D., Peng, C. C., Schenk, J. O., Joswig-Jones, C., and Jones, J. P. (2011) The kinetic mechanism for cytochrome P450 metabolism of type II binding compounds: evidence supporting direct reduction, *Arch. Biochem. Biophys. 511*, 69-79.

For Table of Contents use only